Flexible Electronics

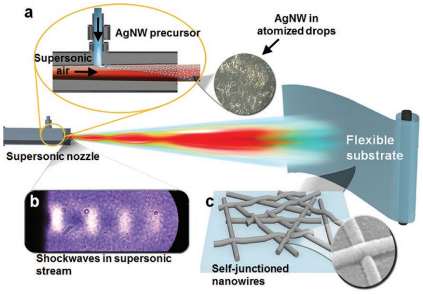

A schematic of supersonic spraying of a silver nanowire (AgNW) film is shown. AgNWs are shown in an optical microscope image. Superdeposited nanowires with a junction are highlighted as a scanning electron microscopy (SEM) image.

ADVANCED FUNCTIONAL MATERIALS
www.afm-journal.de

Production of Flexible Transparent Conducting Films of Self-Fused Nanowires via One-Step Supersonic Spraying

*Jong-Gun Lee, Do-Yeon Kim, Jong-Hyuk Lee, Suman Sinha-Ray, Alexander L. Yarin, Mark T. Swihart, Donghwan Kim, and Sam S. Yoon**

Scalable and economical manufacturing of flexible transparent conducting films (TCF) is a key barrier to widespread adoption of low-cost flexible electronics. Here, a simple, robust, and scalable method of flexible TCF formation using supersonic kinetic spraying is demonstrated. Silver nanowire (AgNW) suspensions are sprayed at supersonic speed to produce self-sintered films of AgNWs on flexible substrates. These films display remarkably low sheet resistance, <10 Ω sq^{-1}, combined with high transmittance, >90%. These electrically conducting, transparent, and flexible coatings can be deposited over a 100 cm^2 area in ≈30 s. Theoretical analysis reveals the underlying physical mechanism behind self-sintering, showing that self-sintering is enabled by the high velocity of impact in supersonic spraying.

1. Introduction

Transparent conducting films (TCFs) have become ubiquitous in optoelectronic devices, including light-emitting diodes (LEDs),[1] organic LEDs,[2] displays,[3] touch screens,[4] solar cells,[5] smart windows,[6] and interactive electronics.[7,8] An inherent challenge in developing high-performance TCFs arises from the incompatibility of high transmittance (T) and low sheet resistance (R_s). Because the same free charge carriers that increase conductivity also interact with light and reduce transmittance, R_s and T are highly correlated. Conducting materials, such as carbon nanotubes (CNTs),[3,9,10] graphene,[4,11–13] metal nanofibers,[14–17] and conducting polymers,[18] that provide low R_s also reduce T.

Currently, indium tin oxide (ITO) is the most widely used material in TCFs. It combines reasonably high performance (i.e., relatively low sheet resistance and high transmittance) with good chemical and mechanical stability. However, the inherent brittleness of ITO makes it inappropriate for use in flexible and stretchable electronics. Moreover, the cost and supply of raw materials for ITO are unstable. This volatility inflicts a financial risk and burden on manufacturers that are reliant on ITO.[19]

To circumvent the shortcomings of ITO, nanomaterials such as CNTs, graphene, and metal nanowires have been suggested as alternative TCF materials in flexible electronics. 1D nanomaterials (CNTs and metal nanowires) can form a mesh-like structure with high transparency. The nanoscale diameter of these materials alters their interaction with light, improving transparency, and allowing mesh-like films to have quasiuniform conductivity at the microscale and above. High theoretical values notwithstanding, the electrical conductivities of CNTs and graphene films are generally much lower than those of metal (copper or silver) nanowires (NWs). The performance of metal NW films is generally limited by high contact resistance between overlapping NWs (junction resistance). Fusion processes, such as pressing and annealing, have been applied to reduce junction resistance.[20] However, pressing often inflicts mechanical damage on the films. Annealing is limited by the thermal stability of the flexible substrate, seriously limiting its applicability in flexible electronics. Thus, an alternative route to fuse junctions of such NWs without sacrificing TCF quality or constraining the choice of substrates remains urgently needed.

In general, achieving visible light transmittance >90% along with sheet resistance below 10 Ω sq^{-1} using silver nanowires has been exceedingly difficult because the percolating network that provides low resistance reduces transmittance.[21] The contact resistance at the NW junctions contributes significantly to the overall sheet resistance, increasing the density of the network of NWs required to achieve a desired low value of R_s. Hsu et al.[22] combined copper microfibers with silver NWs to achieve transmittance >90% and sheet resistance <1 Ω sq^{-1}. In that case, high performance resulted from facile electron

J.-G. Lee, D.-Y. Kim, J.-H. Lee, Prof. A. L. Yarin, Prof. S. S. Yoon
School of Mechanical Engineering
Korea University
Seoul 02841, Republic of Korea
E-mail: skyoon@korea.ac.kr
Dr. S. Sinha-Ray, Prof. A. L. Yarin
Department of Mechanical and Industrial Engineering
University of Illinois at Chicago
842 W. Taylor St., Chicago, IL 60607-7022, USA
Dr. S. Sinha-Ray
Department of Materials Science and Engineering
Indian Institute of Technology
Indore, Madhya Pradesh 452017, India
Prof. M. T. Swihart
Department of Chemical and Biological Engineering
University at Buffalo
The State University of New York
Buffalo, NY 14260-4200, USA
Prof. D. Kim
School of Materials Science and Engineering
Korea University
Seoul 02841, Republic of Korea

DOI: 10.1002/adfm.201602548

transport through the microscopic copper fibers, which yielded low overall sheet resistance with relatively sparse coverage of silver nanowires and copper microfibers. One drawback of this approach might be the multiple steps required for coupling silver nanowires and copper microfibers, not to mention the vacuum deposition processes used as the intermediate steps. An et al.[23] also used copper microfibers and achieved transmittance >97% and sheet resistance <0.42 Ω sq^{-1}, but have not demonstrated large-scale production of the transparent conducting film. For large-scale practical industrial applications, a simple nonvacuum one-step deposition method would be preferable. Moreover, an optimal process would not require any postannealing or pressing process that can damage the film or substrate.[24]

Here, we show that supersonically sprayed silver nanowires can be deposited on flexible substrates at large-scale (here, 36.3 cm long diagonally on a flat substrate or a few meters long on a roll-to-roll film) to form a high performance TCF. Silver nanowires are sprayed at a supersonic speed, and their kinetic energy is converted on impact into thermal energy that allows fusion of the NWs to reduce or eliminate junction resistance. This reduction of junction resistance allows the relationship between light transmittance and sheet resistance to remain linear at high transparency. In most TCFs, the sheet resistance is high at high transparency (T), especially for $T > 90\%$, at which point the linear relationship between the sheet resistance and transparency is distorted and becomes highly nonlinear. However, in our self-fused silver NW films, the linear relation between the sheet resistance and transparency is maintained up to $T = 97\%$. Moreover, this excellent performance persists over numerous bending and stretching cycles.

2. Results and Discussions

Figure 1 illustrates the overall process for producing the silver nanowire (AgNW) films. An AgNW dispersion was supplied to the supersonic nozzle, and solvent was evaporated during flight. Binder-free sparse AgNW films were thus coated on various substrates; see Figure S1 in the Supporting Information. The diameter of the AgNW used here was 20 nm, which is significantly smaller than wavelengths of visible light. Use of deep subwavelength structures minimizes light scattering that could lead to haziness as well as reduced transmittance.[25,26]

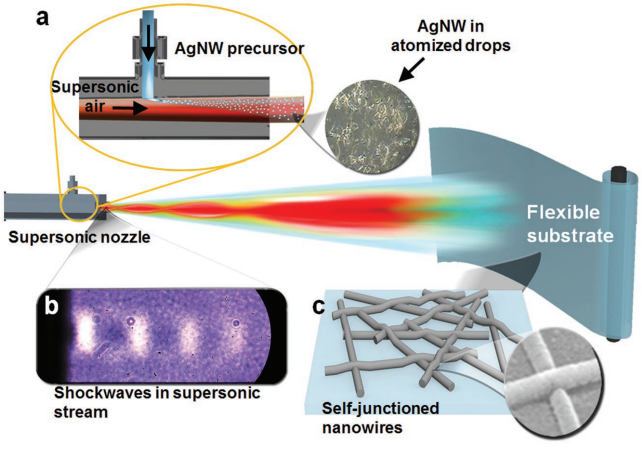

Figure 1. Schematic of the fabrication process of AgNW films. a) Schematic of supersonic spraying of AgNW film. AgNWs are shown in an optical microscope image. b) Shock wave patterns in the supersonic jet used to spray nanowires. c) Superdeposited nanowires with a junction highlighted as an SEM image.

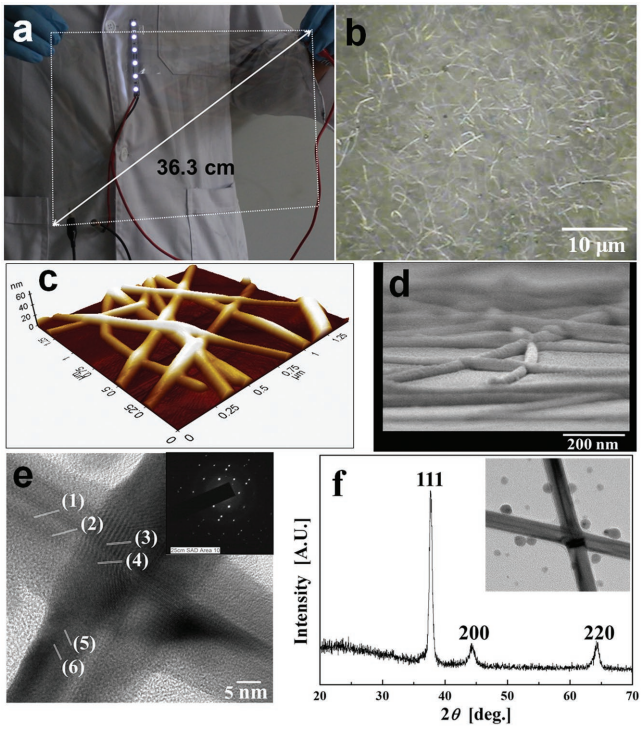

Figure 2. Transparent flexible film of self-fused silver nanowires. a) Photograph of a large-scale AgNW-coated flexible substrate. b) Optical microscope image, c) AFM image, d) SEM image of an AgNW-coated substrate. The SEM image shows that the coating is a monolayer. e) Transmission electron microscopy (TEM) image of two silver nanowires intersecting each other. *Selected area electron diffraction* (SAED) was performed at six locations marked by numerals 1 to 6. The inset shows the SAED pattern from one of these locations. f) The X-ray diffraction pattern of AgNW collected on glass substrate. The peaks correspond to the crystalline planes labeled in the panel.

Figure 2a shows a full-scale flexible substrate coated with AgNWs in 30 s using a single nozzle. The sample size reveals the great potential of the proposed method in terms of manufacturability. Figure 2b provides an optical microscope image (Nikon, Metaphot, Japan) of the coating, showing that it is uniform over the entire field of view. The surface elevations measured using atomic force microscopy (AFM, XE-100, Park systems, Korea) are depicted in Figure 2c. The surface elevations are in the range 0–40 nm, with maximum values at points where multiple silver nanowires overlap. Figure 2d presents an scanning electron microscopy (SEM) image of the coated surface, showing that the AgNWs formed a sparse mesh-like monolayer, and the nanowires were fully fused at their junctions. Figure 2e shows the selected area electron diffraction (SAED) patterns of two nanowires intersecting each other. SAED, which allows resolution of areas of ≈5–10 nm diameter, was performed at the six locations marked in Figure 2e. One SAED pattern is shown in the inset of Figure 2e, but at all six

Adv. Funct. Mater. 2016,
DOI: 10.1002/adfm.201602548

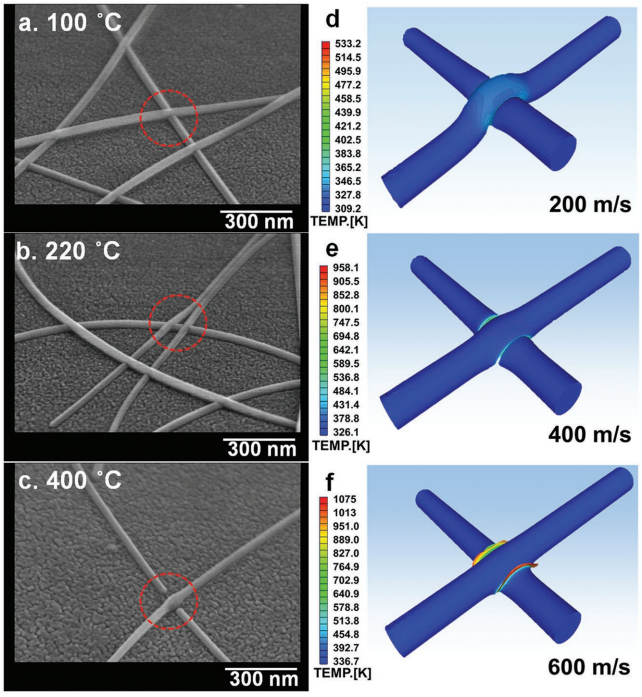

Figure 3. SEM images and simulations of the AgNW-coated flexible substrate for different temperatures of the air entering the supersonic nozzle: a) at 100 °C, b) at 220 °C, and c) at 400 °C. Simulation were performed in Ansys Autodyn. d–f) Simulation results for silver nanowire impact at the indicated impact velocities.

locations, the *d*-spacing of 2.38 Å was consistent with the expected values for Ag (111) planes. A global view of the crystal structure in the coating is provided by X-ray diffraction (XRD) of the AgNWs coated on a glass substrate (Figure 2f). Peaks at 2θ = 37.66°, 43.32°, 64.44°,and 77.64° correspond to the (111), (200), (220), and (311) planes of the face-centered cubic lattice of silver (JCPDS No. 03-0931). The average crystal size from the XRD data based on the (111), (200), (220), (311) planes was 25.4 nm, indicating that crystal domain sizes are limited by the wire diameter (i.e., a single crystal domain spans the width of each wire, as observed in high-resolution transmission electron microscopy (HRTEM)).

Preheating the air entering the supersonic de Laval nozzle increases the air jet velocity, and thus the nanowire impact velocity, and also increases the temperature of the AgNWs. **Figure 3**a–c shows SEM images of the as-deposited silver nanowires on a flexible substrate at different inlet air temperatures. The penetration depth of one silver nanowire into another increases with temperature, with substantial sintering already achieved in the 100–220 °C range (Figure 3a,b). At 400 °C the silver nanowires can cut through one another and separate (Figure 3c), which also increases the electrical resistance. Therefore, further experiments were conducted in the 100–300 °C range. Figure 3d–f shows results of simulations of the impacting silver nanowires and their fusion process upon impact at varying velocities (conducted using Ansys Autodyn, Canonsburg, PA, USA). We varied the operating air pressure and temperature in the range of 1.5–4 bar and 25–400 °C, yielding air velocities of 266–677 m s^{-1} (based on isentropic flow calculations). The silver nanowires entrained into the moving air stream achieve a velocity 10%–20% lower than the air velocity, according to their Stokes number.[27] Thus, we have roughly set the low, medium, and high velocity of the silver nanowires at 200, 400, and 600 m s^{-1}. Fusion is clearly promoted by increasing impact velocity. At the highest impact velocity of 600 m s^{-1}, the nanowire underneath the incoming nanowire was nearly broken into two parts, consistent with the phenomenon observed in Figure 3c.

Figure 4a shows the sheet resistance of supersonically sprayed AgNW achieved using different air temperatures at the entrance to the de Laval nozzle. The results show that an inlet temperature of 220 °C provides the optimum performance, i.e., a lower sheet resistance at higher transmittance. The optimal performance stems from full NW sintering at junctions, which fully eliminates contact resistance (with the sheet resistance being in the 3–10 Ω sq^{-1} range), even though the NW network is very sparse, which allows high light transmittance of 80%–90%. To the best of our knowledge, these are the lowest values of sheet resistance of AgNWs reported at such a high transmittance. Figure 4b shows the extent to which the present

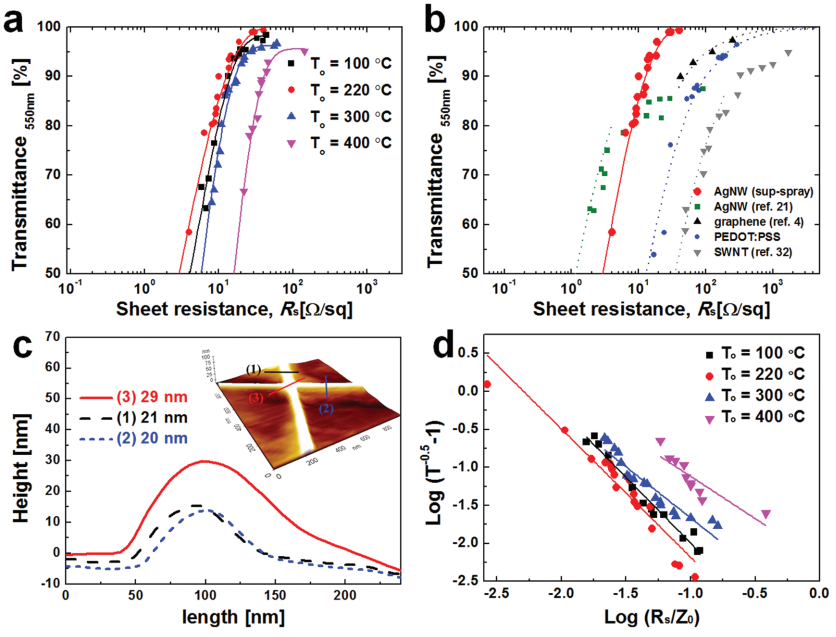

Figure 4. Optical and electrical performance. a) Performance of the supersonically sprayed AgNW film on soda lime glass. Transmittance versus sheet resistance achieved at different temperatures at the entrance to the de Laval nozzle, with the optimal one being 220 °C. b) Comparison of the present transmittance with the results from literature.[4,21,33] c) AFM image of two intersecting AgNWs. d) Figure of merit achieved at different temperatures at the entrance to the de Laval nozzle. All transmittance values are relative to the corresponding uncoated substrate, e.g., for an uncoated substrate absolute transmittance of 90%, and coated substrate absolute transmittance of 85%, the reported transmittance is 0.85/0.90 = 94.4%.

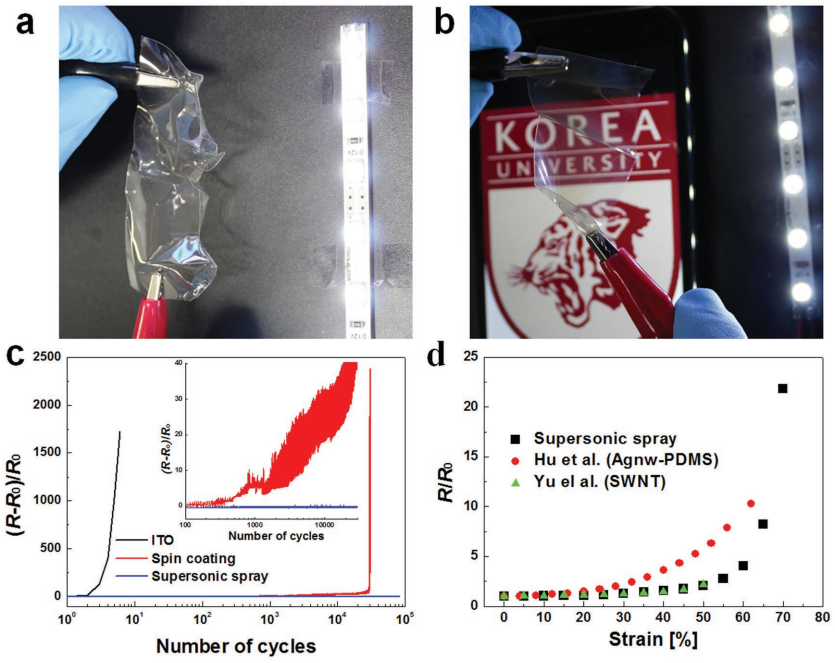

Figure 5. Robustness of the fabricated transparent film. a) It survives extreme mechanical wrinkling and b) bending tests. c) The resistance change ratio versus the number of bending cycles of the present transparent AgNW on a PET substrate compared with that of ITO on PET and spin-coated AgNW on PET. d) Ratio of the sheet resistance change as a function of strain for the AgNW TCF on an Ecoflex substrate, where R_0 is the initial sheet resistance. Results from Hu et al.[34] and Yu et al.[35] are provided for comparison. Note that the transparent film used herein has a sheet resistance of $R_0 = 20\ \Omega\ sq^{-1}$ and transparency of $T = 97\%$.

result outperforms previously reported TCFs. In previous studies using AgNWs with an average length of 2–3 μm, deposited by spin coating and Langmuir–Blodgett techniques, sheet resistance of $R_s \approx 10^3\ \Omega\ sq^{-1}$ and transmittance $T > 80\%$ were obtained.[15,28] Films of longer AgNWs of 6–10 μm produced using vacuum filtration revealed slightly improved values of $R_s \approx 10^2\ \Omega\ sq^{-1}$ and $T > 92\%$.[26] TCFs composed of extremely long AgNWs (≈95 μm) using successive multistep growth yielded $R_s \approx 69\ \Omega\ sq^{-1}$ and $T = 95\%$.[29] These results suggest that increasing AgNW length improves performance of TCFs. However, multiple processing steps were required for long wire fabrication and deposition, and so far, only spin-coating, vacuum filtration (or suction), drop-casting, and doctor blade deposition were employed. An additional mechanical pressing step following drop-coating was introduced to reduce contact resistance at the junctions of the overlapped AgNWs,[30] which reduced sheet resistance to $R_s \approx 8.6\ \Omega\ sq^{-1}$, albeit at a modest transmittance of $T = 80\%$. The usage of such restrictive fabrication methods has limited progress of these AgNW TCFs toward commercialization.

In the present case, the high velocity impact of AgNWs on one another, driven by the supersonic air jet, produces mutual sintering as explained further below. Figure 4c shows direct evidence of AgNW sintering. Although the NW diameter (height measured by AFM) is ≈20 nm, the junction height is only 29 nm, implying partial fusion of the nanowires. In prior studies of NW-based TCFs, the NWs were not sintered, which resulted in high contact resistance. For example, at comparably high transmittance, the sheet resistance measured by De et al.[21] and Garnett et al.[31] was one to two orders of magnitude higher than that reported here. Along with reducing junction resistance, the present work employs relatively long NWs, 10–15 μm in length. The robustness of supersonic spraying ensured that such relatively long NWs could be sprayed without clogging or process interruptions.

The mechanical robustness of the flexible AgNW-coated TCFs formed by supersonic spraying is illustrated in **Figure 5**. Figure 5a,b shows severe deformations of a sample. Still, the AgNW-coated sample retained its conductivity. In Figure 5a,b, a series of LED lights are connected across the AgNW-coated flexible substrates, which were severely folded and wrinkled. Despite severe deformation, there was no variation in the illumination provided by the LED lights. The AgNW-coated samples were compared to ITO-coated flexible substrates and spin-coated AgNW films on a flexible substrate. For that, ITO was sputtered on a flexible polyethylene terephthalate (PET) substrate of 100 μm thickness. The initial sheet resistance of the ITO film was 20 Ω sq^{-1}. Silver nanowires were also spin-coated on a flexible PET substrate to achieve an initial sheet resistance of 12 Ω sq^{-1}. These ITO-coated and AgNW-spin-coated flexible samples were subjected to a bending test (with a bending radius of $R_b = 5$ mm, bending speed of 5 mm s^{-1}, and 8×10^4 cycles) and their performance was compared to that of the supersonically coated AgNW films. For supersonically coated AgNW films, no change in the sheet resistance was observed. On the contrary, the ITO-coated films failed (stopped being electrically conducting) in a few bending cycles, while the spin-coated films sustained conductivity for only 3×10^4 cycles (Figure 5c).

Figure 6 shows results of a stretchability test of AgNWs, which were deposited on an Ecoflex substrate. Both ends of the Ecoflex film were tightly attached to movable holders. An LED light was connected to the stretching film to ensure its electrical conductivity status. The light intensity was unchanged up to 700% strain, beyond which the light intensity began to decrease; see Movie S1 in the Supporting Information. At 720% strain, electrical failure was complete, and the light was no longer illuminated. This record was achieved using relatively short AgNWs (i.e., 20 μm long), while the previous authors has succeeded in stretching up to 460% using very long AgNWs (i.e., 500 μm).[25] Therefore, this achievement of greater stretchability only using shorter AgNWs indicates the superior performance of supersonically sprayed self-fused AgNW transparent flexible films.

Figure 7 shows a large-scale silver nanowire film produced by the roll-to-roll spray coating system depicted in Figure 7a,b. This roll-to-roll film has transparency of 92% and an average

Adv. Funct. Mater. **2016**,
DOI: 10.1002/adfm.201602548

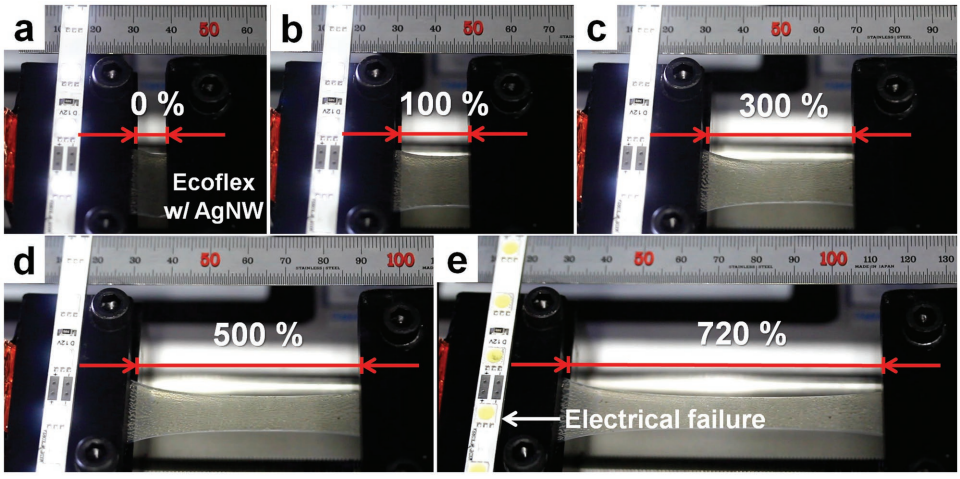

Figure 6. a–e) Stretching test of AgNW films. An Ecoflex substrate spray-coated with AgNWs is stretched beyond 700% of the initial length without loss of conductance. At 720% stretching, electrical continuity was lost and the LEDs turned off.

sheet resistance of R_s = 18 Ω sq^{-1}. Figure 7a is the roller that feeds the flexible PET (polyethylene terephthalate) substrate which is coated across the supersonic "Air" nozzle depicted in Figure 7b. Here, the silver nanowires are fed and entrained into the supersonic air stream and are eventually coated onto the moving PET substrate.

3. Theoretical Estimates

The kinetic energy of impact is evaluated as $\rho V^2 l^3$, where ρ is the silver density, V is the air jet velocity, and l is the volume-equivalent diameter of a NW. The fusion energy is of the order $\rho L l^3$, where L is the specific latent heat of fusion of silver. The energy required to heat the NW to its melting temperature is about $\rho c \Delta T l^3$, where c is the specific heat of silver, and ΔT is the temperature difference between the melting temperature and room temperature. Data for silver show that $\rho c \Delta T l^3 + \rho L l^3 \approx 3\rho L l^3$, which is the total energy required to heat a nanowire up and melt it. With $V \approx$ 200, 400, and 600 m s^{-1}, the ratio of the kinetic energy to the total energy required for melting NW is of the order of $V^2/(3L) \approx$ 0.25, 1, and 2.25, respectively. This means that fusion of two NWs due to the impact of one of them onto the other one already located on the substrate is not expected in the case of the impact velocity of 200 m s^{-1}, while it is expected in the cases of 400 and 600 m s^{-1}. This conclusion is in full agreement with the experimental findings and numerical results shown in Figure 3. In particular, Figure 3d–f predicts that there is no fusion of two NWs after an impact at 200 m s^{-1}, which agrees with the above estimate that the kinetic energy of impact at this velocity comprises only 25% of the energy required to heat the NWs up to their melting temperature and to cause melting, which facilitates fusion. On the contrary, at 400 m s^{-1}, according to the above estimate, the kinetic energy of impact is sufficient for melting and thus fusion, and indeed, the numerically generated Figure 3e reveals that this is the case, consistent with the observation of experimental Figure 3b. The same is true in the case of the impact velocity of 600 m s^{-1}. Moreover, in this case the kinetic energy of impact is 2.25 times higher than the one required to melting and fusion. As a result, Figure 3f reveals an almost complete cutting of the stationary NW by the impacting one, similar to the experimental observation in Figure 3c. Note that melting on impact requires an additional condition to be fulfilled. Namely, the characteristic time for cooling by thermal conduction $\tau_{cond} \approx l^2/\alpha$ should be much longer than the characteristic impact time $\tau_{imp} \approx a/V$, where α is the thermal diffusivity of silver, and a is the cross-sectional radius of a NW. Taking for the estimate α = 1.66 cm^2 s^{-1} and $a \approx$ 20 nm, we find $\tau_{cond} \approx 10^{-8}$ s and $\tau_{imp} \approx 0.5 \times 10^{-10}$ s, which means that $\tau_{imp} << \tau_{cond}$, and the thermal energy will not be lost via thermal conduction during impact, and thus remains available for melting and fusion. The latter estimate is done for the impact velocity of 400 m s^{-1}, but it definitely holds for 200 and 600 m s^{-1}. The fusion time of two molten silver NWs is of the order of $\tau_{fusion} \approx 2\mu a/(3\sigma)$, where μ and σ are the viscosity and surface tension of molten silver. Taking for the estimate μ = 1 cP, and σ = 100 g s^{-2}, we find $\tau_{fusion} = 10^{-9}$ s, i.e., the time scale for melting and fusion is shorter than that

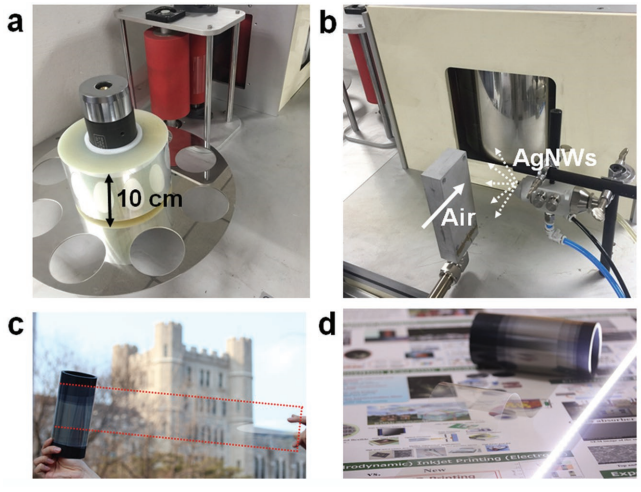

Figure 7. a–d) AgNW films deposited using a roll-to-roll process.

for heat loss by conduction to the substrate (this conclusion is valid for the impact velocities of 200–600 m s^{-1}). It should be emphasized that fusion happens at the contact of two wires, which is heated up due to their collision. The estimates in this section explain the experimental observations in section 2 that revealed fused AgNWs.

4. Conclusions

We have introduced a commercially viable, simple, scalable one-step supersonic spray-coating method to create highly transparent, flexible, rollable, stretchable, and conducting films. This method requires no post-treatment steps, and the fabricated films display remarkably low sheet resistance, <10 Ω sq^{-1}, combined with high transmittance, >90%.

5. Experimental Section

Materials: Two types of commercially available silver nanowires were used. The first (Aiden, Korea) had an average diameter and length of 20 nm and 15 µm, respectively. The second (Cambrios, Clear Ohm) had an average diameter and length of 20 nm and 10 µm. The silver nanowires of the first type were dispersed in isopropyl alcohol at a concentration of 0.15 wt%, while silver nanowires of the second type were dispersed in ethanol at 1 wt%. For the experiments reported here, the dispersions were blended together with isopropyl alcohol (IPA, Duksan, Korea) at weight ratios of 2:1:6 for the nanowire dispersions of the first type, the second type, and IPA, respectively. This mixture was selected as a compromise between the two types of nanowires alone. The Aiden AgNWs were ≈50% longer than the Cambrios AgNWs, which allowed them to provide lower sheet resistance for a given quantity of AgNWs deposited. On the other hand, the Aiden AgNW dispersion contained a significant amount of free Ag nanoparticles, which reduced transparency and increased haziness without contributing much to conductivity. Most free AgNPs had been removed from the Cambrios AgNW dispersion. Perhaps as a result of this extensive purification, the Cambrios AgNW dispersion was approximately ten times the cost of the Aiden NW dispersion. In summary, the Aiden AgNW produced lower sheet resistance films, but their transparency was not as good because of the presence of excess AgNPs. On the other hand, the Cambrios AgNWs produced more transparent films with somewhat higher sheet resistance. Thus, to balance the advantages and disadvantages of these AgNW precursors, a 2:1 mass ratio of Aiden to Cambrios AgNWs was employed in all experiments reported here.

Experimental Procedure: A schematic of the apparatus and process used for producing NW TCFs is shown in Figure 1a. The silver nanowire dispersion (AgNW dispersion) was injected at an experimentally optimized location within the de Laval nozzle at a flow rate of 1.2 mL min^{-1} using a syringe pump (Legato 210, KDS). The AgNW dispersion was atomized by the supersonic air jet issued from the de Laval nozzle operating pressure in the range of 1.5–4 bar at several different temperatures of the air entering the nozzle: room temperature, 100, 220, 300, and 400 °C. Figure 1b shows an experimentally observed Schlieren-photography pattern of shock waves in the near-field of the supersonic jet during a typical spraying process. During flight, the solvent fully evaporated from the dispersion droplets and only AgNWs were deposited onto the target flexible substrate.[32] The motorized stage on which the substrate was placed could move at a scanning speed of 4 cm s^{-1} in two orthogonal *x*–*y* directions to allow formation of a large-area film with the nozzle fixed and stationary. In general, coating an area of 30.2 × 20.2 cm^2 required ≈30 s using this lab-scale system with a single nozzle. An array of such nozzles could allow rapid production of such coatings on wide substrates in a roll-to-roll process.

Supporting Information

Supporting Information is available from the Wiley Online Library or from the author.

Acknowledgements

J.-G.L. and D.-Y.K. contributed equally to this work. This research was supported by the National Research Foundation GFHIM-2013M3A6B1078879 and the Industrial Strategic Technology Development Program (10045221) funded by the Ministry of Knowledge Economy (MKE, Korea).

Received: May 23, 2016
Revised: September 4, 2016
Published online:

[1] L. Li, Z. Yu, W. Hu, C. h. Chang, Q. Chen, Q. Pei, *Adv. Mater.* **2011**, *23*, 5563.
[2] J. Wu, M. Agrawal, H. A. Becerril, Z. Bao, Z. Liu, Y. Chen, P. Peumans, *ACS Nano* **2009**, *4*, 43.
[3] D. S. Hecht, L. Hu, G. Irvin, *Adv. Mater.* **2011**, *23*, 1482.
[4] S. Bae, H. Kim, Y. Lee, X. Xu, J.-S. Park, Y. Zheng, J. Balakrishnan, T. Lei, H. R. Kim, Y. I. Song, *Nat. Nanotechnol.* **2010**, *5*, 574.
[5] Z. Yu, L. Li, Q. Zhang, W. Hu, Q. Pei, *Adv. Mater.* **2011**, *23*, 4453.
[6] S. K. Deb, S.-H. Lee, C. E. Tracy, J. R. Pitts, B. A. Gregg, H. M. Branz, *Electrochim. Acta* **2001**, *46*, 2125.
[7] D. J. Lipomi, M. Vosgueritchian, B. C. Tee, S. L. Hellstrom, J. A. Lee, C. H. Fox, Z. Bao, *Nat. Nanotechnol.* **2011**, *6*, 788.
[8] H. Peng, W. Dang, J. Cao, Y. Chen, D. Wu, W. Zheng, H. Li, Z.-X. Shen, Z. Liu, *Nat. Chem.* **2012**, *4*, 281.
[9] Z. Wu, Z. Chen, X. Du, J. M. Logan, J. Sippel, M. Nikolou, K. Kamaras, J. R. Reynolds, D. B. Tanner, A. F. Hebard, *Science* **2004**, *305*, 1273.
[10] M. Zhang, S. Fang, A. A. Zakhidov, S. B. Lee, A. E. Aliev, C. D. Williams, K. R. Atkinson, R. H. Baughman, *Science* **2005**, *309*, 1215.
[11] K. S. Kim, Y. Zhao, H. Jang, S. Y. Lee, J. M. Kim, K. S. Kim, J. H. Ahn, P. Kim, J. Y. Choi, B. H. Hong, *Nature* **2009**, *457*, 706.
[12] G. Eda, G. Fanchini, M. Chhowalla, *Nat. Nanotechnol.* **2008**, *3*, 270.
[13] X. Li, G. Zhang, X. Bai, X. Sun, X. Wang, E. Wang, H. Dai, *Nature Nanotechnol.* **2008**, *3*, 538.
[14] A. R. Rathmell, B. J. Wiley, *Adv. Mater.* **2011**, *23*, 4798.
[15] P. C. Hsu, S. Wang, H. Wu, V. K. Narasimhan, D. Kong, H. R. Lee, Y. Cui, *Nat. Commun.* **2013**, *4*, 1.
[16] S. Soltanian, R. Rahmanian, B. Gholamkhass, N. M. Kiasari, F. Ko, P. Servati, *Adv. Energy Mater.* **2013**, *3*, 1332.
[17] H. Wu, D. Kong, Z. Ruan, P.-C. Hsu, S. Wang, Z. Yu, T. J. Carney, L. Hu, S. Fan, Y. Cui, *Nat. Nanotechnol.* **2013**, *8*, 421.
[18] M. Vosgueritchian, D. J. Lipomi, Z. Bao, *Adv. Funct. Mater.* **2012**, *22*, 421.
[19] F. Wong, M. Fung, S. Tong, C. Lee, S. Lee, *Thin Solid Films* **2004**, *466*, 225.
[20] L. Hu, H. S. Kim, J.-Y. Lee, P. Peumans, Y. Cui, *ACS Nano* **2010**, *4*, 2955.
[21] S. De, P. J. King, P. E. Lyons, U. Khan, J. N. Coleman, *ACS Nano* **2010**, *4*, 7064.
[22] P. C. Hsu, S. Wang, H. Wu, V. K. Narasimhan, D. Kong, H. R. Lee, Y. Cui, *Nat. Commun.* **2013**, *4*, 2522.
[23] S. An, H. S. Jo, D.-Y. Kim, H. J. Lee, B.-K. Ju, S. S. Al-Deyab, J. H. Ahn, Y. Qin, M. T. Swihart, A. L. Yarin, S. S. Yoon, *Adv. Mater.* **2016**, *28*, 7149.

[24] J. A. Spechler, K. A. Nagamatsu, J. C. Sturm, C. B. Arnold, *ACS Appl. Mater. Interfaces* **2015**, *7*, 10556.
[25] P. Lee, J. Lee, H. Lee, J. Yeo, S. Hong, K. H. Nam, D. Lee, S. S. Lee, S. H. Ko, *Adv. Mater.* **2012**, *24*, 3326.
[26] S. De, T. M. Higgins, P. E. Lyons, E. M. Doherty, P. N. Nirmalraj, W. J. Blau, J. J. Boland, J. N. Coleman, *ACS Nano* **2009**, *3*, 1767.
[27] M. W. Lee, J. J. Park, D. Y. Kim, S. S. Yoon, H. Y. Kim, D. H. Kim, S. C. James, S. Chandra, T. Coyle, J. H. Ryu, W. H. Yoon, D. S. Park, *J. Aerosol Sci.* **2011**, *42*, 771.
[28] A. Tao, F. Kim, C. Hess, J. Goldberger, R. He, Y. Sun, Y. Xia, P. Yang, *Nano Lett.* **2003**, *3*, 1229.
[29] J. Lee, P. Lee, H. Lee, D. Lee, S. S. Lee, S. H. Ko, *Nanoscale* **2012**, *4*, 6408.
[30] T. Tokuno, M. Nogi, M. Karakawa, J. Jiu, T. T. Nge, Y. Aso, K. Suganuma, *Nano Res.* **2011**, *4*, 1215.
[31] E. C. Garnett, W. Cai, J. J. Cha, F. Mahmood, S. T. Connor, M. G. Christoforo, Y. Cui, M. D. McGehee, M. L. Brongersma, *Nat. Mater.* **2012**, *11*, 241.
[32] D. Y. Kim, S. Sinha-Ray, J. J. Park, J. G. Lee, Y. H. Cha, S. H. Bae, J. H. Ahn, Y. C. Jung, S. M. Kim, A. L. Yarin, S. S. Yoon, *Adv. Funct. Mater.* **2014**, *24*, 4986.
[33] V. Scardaci, R. Coull, J. N. Coleman, *Appl. Phys. Lett.* **2010**, *97*, 023114.
[34] W. Hu, X. Niu, L. Li, S. Yun, Z. Yu, Q. Pei, *Nanotechnology* **2012**, *23*, 344002.
[35] Z. Yu, X. Niu, Z. Liu, Q. Pei, *Adv. Mater.* **2011**, *23*, 3989.